Thin Organic-Inorganic Anti-Fouling Hybrid-Films for Microreactor Components

Vanessa Neßlinger, Stefan Welzel, Florian Rieker, Dennis Meinderink, Ulrich Nieken, and Guido Grundmeier*

Deposit formation and fouling in reactors for polymer production and processing especially in microreactors is a well-known phenomenon. Despite the flow and pressure loss optimized static mixers, fouling occurs on the surfaces of the mixer elements. To improve the performance of such parts even further, stainless steel substrates are coated with ultra-thin films which have low surface energy, good adhesion, and high durability. Perfluorinated organosilane (FOTS) films deposited via chemical vapor deposition (CVD) are compared with FOTS containing zirconium oxide sol-gel films regarding the prevention of deposit formation and fouling during polymerization processes in microreactors. Both film structures led to anti-adhesive properties of microreactor component surfaces during aqueous poly(vinylpyrrolidone) (PVP) synthesis. To determine the morphology and surface chemistry of the coatings, different characterization methods such as X-ray photoelectron spectroscopy (XPS) and Fourier transform infrared (FTIR) spectroscopy as well as microscopic methods such as field-emission scanning electron microscopy (FE-SEM) and atomic force microscopy (AFM) are applied. The surface free energy and wetting properties are analyzed by means of contact angle measurements. The application of thin film-coated mixing elements in a microreactor demonstrates a significant lowering in pressure increase caused by a reduced deposit formation.

V. Neßlinger, F. Rieker, D. Meinderink, G. Grundmeier
Paderborn University
Faculty of Science
Department of Chemistry
Technical and Macromolecular Chemistry (TMC)
Warburger Str. 100, 33098 Paderborn, Germany
E-mail: g.grundmeier@tc.uni-paderborn.de
S. Welzel, U. Nieken
Institute of Chemical Process Engineering
University of Stuttgart
Böblinger Str. 78, 70199 Stuttgart, Germany

1. Introduction

The production of poly(vinylpyrrolidone) (PVP) mainly takes place in batch and semi-batch process operations in tank reactors. Since smart scale reactors such as tubular reactors with static mixing elements are in the focus of interest due to process intensification and energy reduction, extensive experimental investigations have been carried out in such systems.[1,2] Continuous reactor operation allows for better controllability, larger volume to surface ratio, better heat transfer, and good scalability from laboratory to the production plant. The main drawback in the application of continuous reactors for PVP polymerization is the formation of gel deposits. This results in blocking of the cross-sectional area, a strong increase of pressure drop, and subsequently in reactor shutdown.[2,3]

The formation of deposits and polymer fouling is a known challenge in many industrial applications, such as membrane and filtration technologies,[4,5] bio-fouling in the context of silicon and silicon-based materials,[6] and food engineering/protein fouling.[7–9] The formation of polymeric deposits seems to take place especially at the liquid/metal oxide interface, where the preferable tendency of PVP to form complexes with proton donors could be of importance.[10]

One of the main difficulties is to correlate the fouling characteristics with the polymerization mechanism. In this regard, it was shown that high molecular weight and branched or crosslinked polymers are produced by side reactions and play an important role in the occurrence of fouling.[11–13] However, a systematic understanding of how polymer fouling contributes to polymerization and vice versa is still lacking.

Most studies in the field of fouling mitigation focus on anti-adhesive coatings and materials.[14–17] According to Malayeri et al.,[18] besides an increase of the wall shear stress, which is difficult to implement in most industrial processes, a reduction of adhesion work occurring between the surface and the fouling agents can significantly influence fouling deposition processes. Therefore, novel anti-adhesive films should reduce surface roughness and decrease surface free energy.[19] Whereas µm-scaled coatings based on metal-nitrides, such as Cr_xAl_yON or Ti_xAl_yON, are reported to combine enhanced wear resistance and

**ADVANCED
SCIENCE NEWS**

www.advancedsciencenews.com

acro-
olecular

Reaction Engineering
www.mre-journal.de

thermal stability with anti-adhesive properties in injection molding processes,[20–24] other hydrophobic films with low surface energy are promising regarding anti-fouling properties during polymerization in reactors. In this regard, especially perfluorinated organosilanes (FOTS) have received considerable attention lately, not only because of the high thermal and chemical stability due to the carbon (C)-fluorine (F) bond strength[25] (binding energy 485.7 kJ mol^{-1}[26]) but also because of the reduced polarizability of the C–F bond which limits their susceptibility of van der Waals attractive interactions and finally results in low interactions with other materials.[27]

A considerable amount of literature has been published on coatings with perfluorinated molecules.[28–30] It is known that a higher fluorine content, in general, leads to a higher chemical and thermal stability, an increased resistance against solvents as well as a lower surface water wettability. Some studies have investigated the interactions between the coating and functional groups of a polymeric fluid. For instance, according to studies from Al-Harbi et al.,[10] hydrogen bonds, formed between the oxygen of the carbonyl group (C=O) of PVP and the hydrogen of surface silanol groups, are responsible for binding onto OH-terminated surfaces, such as silica. C–F bonds, and therefore fluorine-presenting surfaces, are no good hydrogen bonding acceptors or π-donors and the interactions of fluorine with its environment are mainly of electrostatic nature,[31] which makes them suitable for PVP anti-fouling films.

Furthermore, water present at the solid/liquid interface is suspected to support polymer adsorption onto metal oxides.[32] Water-repellant characteristics are therefore of fundamental importance for anti-adhesive coatings. In this regard, Zisman et al.[33] showed the influence of the outermost surface structure on the hydrophobicity and determined the surface tension to be dependent on the constituent group, which makes the named value to descend in the order –CH$_2$, –CH$_3$, –CF$_2$, –CF$_3$. These observations explain the slightly lower water contact angle generally reported for PTFE coatings (for instance 108° on silica[34]) in contrast to comparable surfaces coated with perfluoroalkyl silanes (for instance 121° on silica[35]). It is even reported that a 2.5–3.3 times decrease of the surface energy is obtained by coating a metal with a perfluoroalkyl silane in comparison to the bare substrate.[36] Despite the length of the perfluoroalkyl chain, where an increased chain length leads to a slightly increased water contact angle as demonstrated by Hozumi et al.,[37] also a highly ordered, close-packed array of –CF$_3$ groups is largely responsible for lowering the surface free energy.[33,38]

Perfluorinated molecules offer several possibilities for application methods.[30,39–41] Chemical and physical vapor deposition techniques (CVD, PVD) leading to few nanometer thin films are of particular importance, since tool surfaces with complex geometries, such as components used in microreactors, exhibit micro- or nanostructured surfaces that need to be preserved during the coating procedure. In addition, coatings with a thickness of several micrometers offer the risk for undesired film infiltration, which finally leads to delamination or peel-off within the process. However, the sol-gel technology offers the opportunity to deposit very thin films with high barrier properties. Advantages such as low-temperature and simple processing are widely reported for such films and enable the formation of smooth and homogeneously coated multi-component surfaces[42,43] that com-

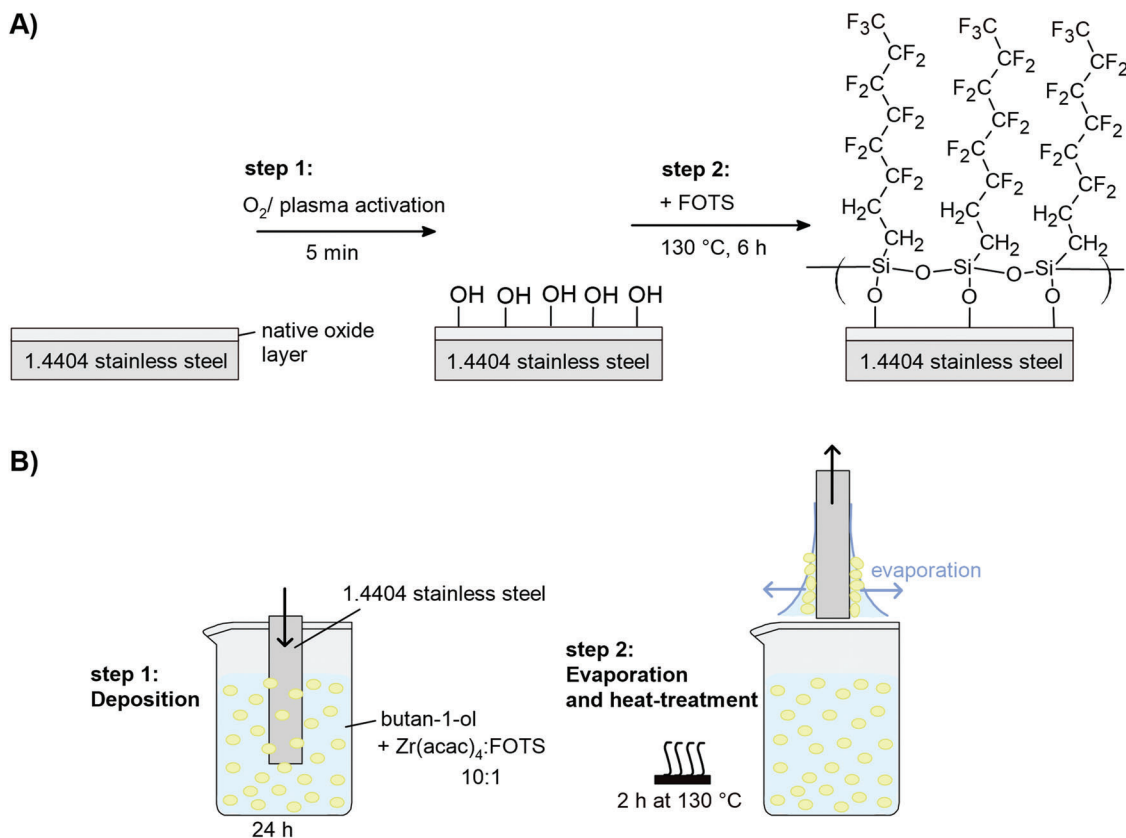bine properties of the inorganic and organic components based on the formation of a stable cross-linked structure.[44]

In this regard, Oldani et al.[19] presented a perfluoropolyether coating on heat exchangers with an improvement of heat-transfer properties ≈10% due to less CaSO$_4$-fouling, in comparison to the use of uncoated material. Further, Kwon et al.[45] demonstrated considerable fouling mitigation against proteins and polymer nanoparticles by applying a fluoropolymer coating on gold surfaces. Lately, also hybrid or multilayer films formed by ceramic oxides such as TiO$_2$ and ZrO$_2$[25] or NiO[29] in combination with fluoropolymers are reported with the aim of fouling protection or the use in injection molding tools, respectively. Zirconium oxides exhibit inert properties with superior thermal stability and large oxidation resistance[46] which makes them a promising candidate for hybrid anti-adhesive coatings in microreactors. Indeed, anti-corrosion properties could be improved by incorporating poly(methylmethacrylate) into a ZrO$_2$-network by sol-gel method.[47]

Based on the necessity for economy and resource conservation, this research study examines the emerging role of the application and the efficiency of two hydrophobic coatings regarding polymeric fouling in real microreactor systems by using the radical polymerization of N-vinylpyrrolidone to PVP in aqueous solution. An ultra-thin FOTS coating is applied to industry relevant 1.4404 stainless steel parts by CVD. Moreover, a thin organic-inorganic hybrid film consisting of zirconium oxide and a FOTS is employed by sol-gel method to combine the inert properties of the metal oxide with the anti-adhesive characteristics of the perfluorinated compound. Surface characterizations by means of X-ray photoelectron spectroscopy (XPS), Fourier transform infrared (FTIR) spectroscopy, and microscopic methods such as field-emission scanning electron microscopy (FE-SEM) and atomic force microscopy (AFM) was performed. An analysis of the surface hydrophobicity and the determination of the surface free energy (SFE) was carried out by means of contact angle measurements. The stability of the ultra-thin surface coatings and the correlation of anti-adhesive properties depending on the surface roughness and morphology could be shown for both polished and cold-rolled stainless steel substrates. The anti-adhesive properties were tested in a lab-scale tubular reactor equipped with untreated and coated stainless steel static mixers under reaction conditions.

2. Experimental Section

2.1. Materials and Chemicals

Chromium-nickel-molybdenum stainless steel substrates (type 1.4404, X2CrNiMo17-12-2, cold-rolled 2B) (referred to as non-polished stainless steel (nps) below) were supplied from Marcegaglia (Italy) and polished stainless steel sheets (type 1.4404, referred to as polished stainless steel (ps) below) from Ullner (Germany) were used. All substrates were subjected to solvent cleaning, consistent of consecutively rinsing in tetrahydrofuran (THF, p.a. grade, stabilized), acetone (p.a. grade), propan-2-ol (p.a. grade), and ethanol (p.a. grade) in an ultrasonic bath for 30 min each. Afterward the samples were dried in a nitrogen stream. All solvents for the cleaning procedure were supplied from Sigma Aldrich (Germany). For the CVD-process

**ADVANCED
SCIENCE NEWS**

www.advancedsciencenews.com

**[M]acro-
molecular
Reaction Engineering**

www.mre-journal.de

Figure 1. Chemical vapor deposition (CVD) process to apply hydrophobic FOTS layer on 1.4404 stainless steel substrates A) includes hydroxylation by plasma treatment (Step 1), condensation, and cross-linking (Step 2) as well as the principle of the dip-coating process to apply the ZrO$_x$/FOTS film onto 1.4404 substrates B) via sol-gel method.

and generation of the hybrid coating 1H,1H,2H,2H-Perfluorooctyltriethoxysilane (FOTS, 98%) from Sigma Aldrich (Germany) was used. Zirconium(IV)-acetylacetonate (Zr(acac)$_4$, 97%, for synthesis) was utilized as a metal-organic precursor and butan-1-ol (anhydrous, 99.8%) was employed for the dip-coating process, both purchased from Sigma Aldrich (Germany).

N-Vinylpyrrolidone (NVP) has been supplied by BASF SE (Germany) in 30 kg barrels stabilized with 0.5% NaOH. The monomer was distilled under vacuum at a temperature of 81–83 °C in the column head to remove the stabilizer and high-molecular components. Afterward the monomer was frozen. The needed amount was defrosted again at the day of the experiment.

2,2'-Azobis[2-methylpropionamidine]dihydrochloride (V-50) was used as an initiator and has been obtained from WAKO chemicals (Germany). It was stored in a fridge and used as delivered.

0.05 mol I2/l – 0.1 N Iodine solution was used as an indicator for PVP on surfaces and has been obtained by Carl Roth GmbH + Co. KG (Germany).

2.2. Thin Film Deposition Processes

The described hydrophobic thin films were applied to: I) flat 1.4404 non-polished (nps), II) polished (ps) stainless steel substrates and III) stainless steel mixing elements.

The hydrophobic FOTS layer was applied to the substrates by means of CVD according to the procedure proposed by Hozumi et al.[37] Therefore, a plasma cleaning step (Plasma Surface Technology, Diener electronic GmbH) was carried out by treating the surfaces in an oxygen plasma ($p < 0.6$ mbar, $>40\,l\,h^{-1}$) for 5 min (compare **Figure 1**A, Step 1). Due to the formation of ozone by excitation of O$_2$ molecules, a photochemical decomposition of organic surface contaminants occurs, which was reported in the literature[48] and evident from XPS analysis, where a distinct decrease in the carbon to iron ratio as well as a decrease of the nitrogen species was measured after the plasma treatment (Figure S1A,C, Supporting Information). Further, a hydroxylated surface was slightly indicated by XPS analysis (Figure S1B, Supporting Information) and was assumed with consideration of the literature.[37,49] The water contact angles were determined directly after the plasma treatment and confirmed a comparable hydrophilicity of the surfaces. Therefore, this procedure leads to a hydrophilic surface with a water contact angle below 10° for both the non-polished and polished 1.4404 substrate. Subsequently, the samples were placed in a PTFE container together with a glass cup filled with 0.2 ml FOTS. The vessel was sealed with a cap and placed in an oven maintained at 130 °C for 4 h. Afterwards the container was opened and stored in the oven at 130 °C for 2 h to allow condensation reaction (Figure 1A, summarized in Step 2). The successful deposition of the FOTS layer was verified by water contact angle (Table 3) and XPS measurements (Figure 4).

ADVANCED
SCIENCE NEWS
www.advancedsciencenews.com

Macro-molecular
Reaction Engineering
www.mre-journal.de

The FOTS-containing ZrO_x films were applied to 1.4404 substrates by sol-gel method, with the procedure being derived from Izumi et al.[28] The coating solution for the dip-coating procedure was prepared by dissolving the appropriate amount of $Zr(acac)_4$ in butan-1-ol to give a final concentration of 50 mmol l^{-1}. While stirring, FOTS was added with a concentration of 5 mmol/l in the final solution. Therefore the $Zr(acac)_4$:FOTS ratio equals to 10:1. The samples were immersed into the freshly prepared solution with a speed of 30 mm s^{-1} without further surface pre-treatment (Figure 1B, Step 1). After 24 h under stirring at room temperature, the samples were pulled out with a velocity of 100 mm s^{-1}. After drying, a 2 h heat-treatment, performed in an oven maintained at 130 °C, completed the surface modification (Figure 1B, Step 2). By using a dip-coater (DC Multi – 8, Nima Technology Ltd) for the overall coating procedure, constant immersion and pull-out rates were ensured. All described sample analysis were performed subsequently after the sample preparation for both described coating procedures and surfaces.

2.3. Surface and Thin Film Analysis

2.3.1. X-Ray Photoelectron Spectroscopy (XPS)

X-ray photoelectron spectroscopy (XPS) was performed using an Omicron ESCA+ system (Omicron NanoTechnology GmbH) equipped with a hemispherical energy analyzer at a base pressure of $<1 \times 10^{-9}$ mbar. Spectra were recorded at pass energies of 100 eV for survey spectra and 20 eV for element spectra. A monochromatic Al Kα (1486.3 eV) X-ray source with a spot diameter of 0.6 mm was used. The take-off angle of the detected photoelectrons was set at 30° in relation to the surface plane. Spectra were internally calibrated to the C1s peak (binding energy 285.0 eV). Peak fitting and data analysis were performed with CasaXPS software (V 2.3.23, Casa Software Ltd.). Quantifications were performed through the integration of the peaks with respect to the corresponding relative sensitivity factor values. A Shirley type background correction and a Gaussian Lorentzian peak shape (70%/30%) were used to fit the measured peaks.

2.3.2. Microscopic Analysis

AFM imaging was performed using a JPK Nanowizard (Bruker Optics GmbH) equipped with an acoustic enclosure in alternating contact mode operating in ambient air conditions at a scan rate of 0.5–1.2 Hz. To this end, HQ:NSC18/AlBS cantilevers (75 kHz and 2.8 N m^{-1}, nominal radius of 8 nm, Mikro-Masch) were used. For subsequent data processing and calculation of root-mean-square (rms)-values for determination of surface roughness, the Gwyddion open source software[50] (V 2.56, Gwyddion) was employed. For the calculation of roughness parameters, at least one position on three distinct, but identically prepared surfaces were analyzed.

Field-emission scanning electron microscopy (FE-SEM) images were obtained by means of a NEON 40 FE-SEM microscope (Carl Zeiss SMT AG), which was equipped with an InLens detector and a SE2. Images were recorded with different magnifications and a tilt angle of 0° and 36° as indicated under the respective figures.

2.3.3. Ellipsometry

The determination of the coating layer thicknesses was performed by using an ellipsometer Accurion Nanofilm EP3 (Accurion GmbH) equipped with a xenon lamp and a mounted 5x objective. Two-zone measurements were performed in a wavelength range from 363.7 nm to 905.9 nm by using a 0–40 filter range with a measurement every second filter. All measurements were performed under ambient air conditions. Data fitting was carried out using the EP4 software. Optical model systems consisting of two consecutive layers were constructed. In the case of the metal oxide, a solvent cleaned 1.4404 ps substrate was measured and served as a reference as underlying reflecting material. Si(100) was selected from the software library for the coating deposition on the silicon wafer. The FOTS-film and the native SiO_2 layer are assumed to be transparent at the wavelength with the same refractive index of 1.46.[37] While this allows direct determination of the FOTS layer thickness on 1.4404 ps, the FOTS-layer thickness on the silicon wafer was achieved by subtracting the native oxide thickness, which was defined to be constant at 1.5 $\pm$ 0.1 nm according to prior measurement, from the total.

A root-mean-square error (rmse) value of <2 was obtained for all measured samples.

2.3.4. Contact Angle Measurements

Static contact angle and free surface energy measurements were carried out with an OCA 15 plus (Dataphysics) at 25 °C using the sessile drop method. For each measurement 5 µl water droplets were dispensed onto the respective surface using a motor-driven syringe, followed by an evaluation with the Laurentian method. Ultrapure water (Carl Roth GmbH) with a dispersive component (γd) of 21.8 mN m^{-1} and a polar component (γp) of 51.0 mN $m^{-1[51]}$ was used for the determination of the static contact angle. As not stated elsewhere, three distinct but identically prepared surfaces were measured for statistical error calculation. Additional liquids with known surface tensions, namely Diiodmethan (for synthesis, Merck, γd: 50.8 mN m^{-1}, γp: 0 mN $m^{-1[51]}$) and Dimethyl sulfoxide (DMSO, >99.9%, Sigma-Aldrich, γd: 34.9 mN m^{-1}, γp: 8.7 mN $m^{-1[52]}$) were selected in order to estimate the total surface free energy (composed of polar and dispersive components) of the coated samples. The OWRK method[53] was applied for evaluation. The standard error was calculated from measuring three drops on three distinct, but identically prepared surfaces each. The sessile drop needle-in method was employed for the dynamic measurements. A volume of 8 µl was placed on the surface and the advancing and receding contact angles were determined by subsequently increasing and decreasing the volume by 5 µl for five times.

2.3.5. Fourier Transform Infrared (FTIR) Spectroscopy

A Vertex 70 spectrometer with an attached Hyperion 1000 microscope (Bruker Corporation) was used for the FTIR measurements. All spectra were recorded in a wavenumber range from 4000 cm^{-1} to 600 cm^{-1} with a resolution of 4 cm^{-1} and a mounted 15x objective in 90° reflection. For a good signal-to-noise ratio, 512 individual spectra were recorded and averaged for each
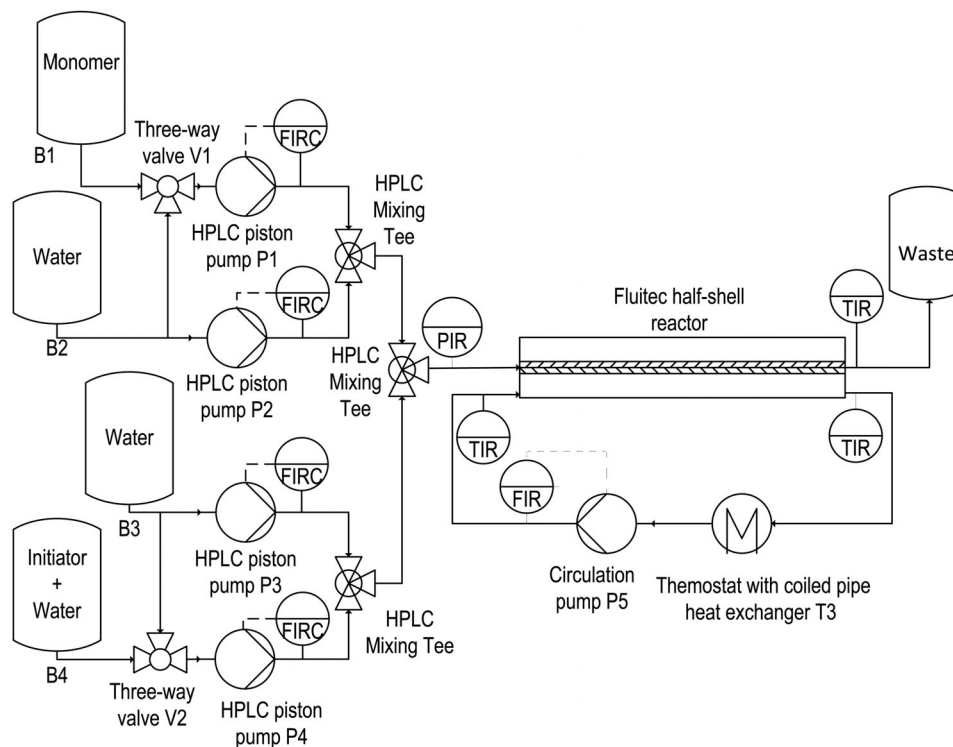
Figure 2. Flow chart of the experimental setup with the Fluitec ContiPlant half-shell reactor.

Table 1. Mass fluxes and composition for the reference case conditions and a superficial velocity of 5 mm s^{-1} in the Fluitec ContiPlant half-shell reactor.

Feed pump	Mass flux/g min^{-1}	Weight fractions (NVP/water/initiator)
P1	6.2	1 / 0 / 0
P2	9.3	0 / 1 / 0
P3	9.3	0 / 1 / 0
P4	6.2	0 / 0.999 / 0.001

spectrum. Appropriate 1.4404 stainless steel substrates served as reference and the OPUS software (V6.5 Bruker Optics GmbH) was used for further data treatment. The latter includes a 1st-order polynomial baseline correction with 6 user-defined baseline points positioned at the same wavenumbers in all cases.

2.4. Experimental Setup for Polymerization in Microreactor

The experimental setup for testing the new coatings on static mixing elements under reaction conditions is shown in **Figure 2**. Four storage containers named B1 to B4 (Figure 2) were prepared with the degassed monomer, the solvent, and an initiator solution as specified in **Table 1**. The feed streams were pumped by Knauer HPLC piston pumps P1 to P4 and controlled by employing Bronkhorst Coriolis mass flow meters and PI controllers. The mass flow rates are given in Table 1 for the reference conditions, which results in a superficial velocity of 5 mm s^{-1}. The feed streams of P1 and P2 as well as those of P3 and P4 have been premixed using 1/16″ HPLC T-connectors and are mixed again

with a 1:1 mass flux ratio in a second 1/16″ HPLC T-connector to ensure a good micro-mixing quality.

The reactor system was heated using a water circuit including the circulation pump P5 and a coiled pipe heat exchanger, which has been placed in an oil bath thermostat (T3). A circulation flux between 7 and 8 l min^{-1} and an oil bath temperature of 100 °C was chosen to adjust a temperature of the heating medium of 86 °C at the reactor inlet. The temperature drops in the water circuit ≈1 °C due to heat losses. At the start of the experiment the reactor was flooded with the monomer-water solution, then the initiator-water solution was added.

The reactor system consists of one Fluitec ContiPlant half-shell reactor with an internal diameter of 12.3 mm and a length of 495 mm. The tested geometry of the static mixing elements is the flow and pressure-loss optimized Fluitec CSE-XD6 (**Figure 3**).
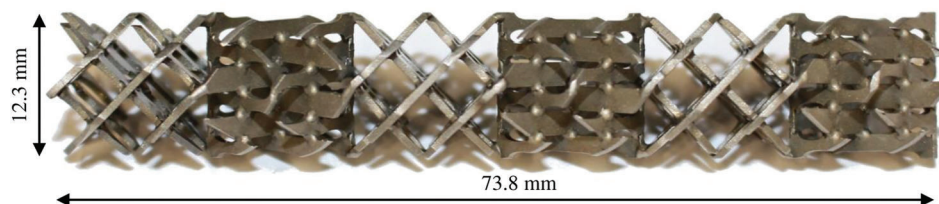
In each experiment 7 coated or uncoated static mixer elements were placed into the reactor, respectively. In the reactor outlet, a small flat plate with the same surface composition as the static mixers was mounted for offline characterization. The operation time of each run was 10.25 h. Due to the appearance of deposits only after a certain time on factory-fresh uncoated mixers, each experiment was carried out several times.
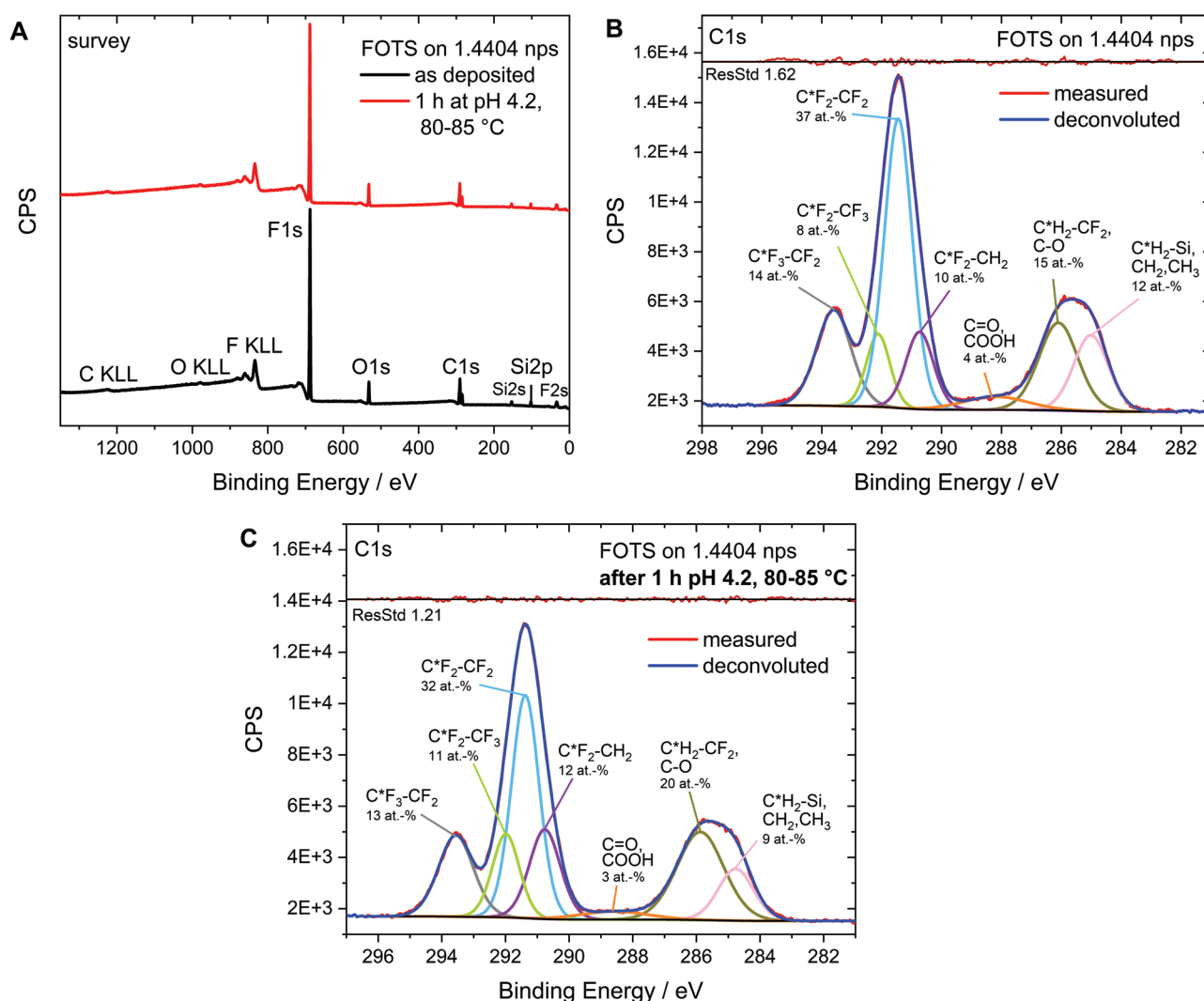
3. Results and Discussion

3.1. Surface and Thin Film Characterization

3.1.1. Surface Composition

XPS measurements were carried out to analyze the reference surface states and coatings on a molecular level as well as to

**ADVANCED
SCIENCE NEWS**

www.advancedsciencenews.com

Macro-
molecular
Reaction Engineering

www.mre-journal.de

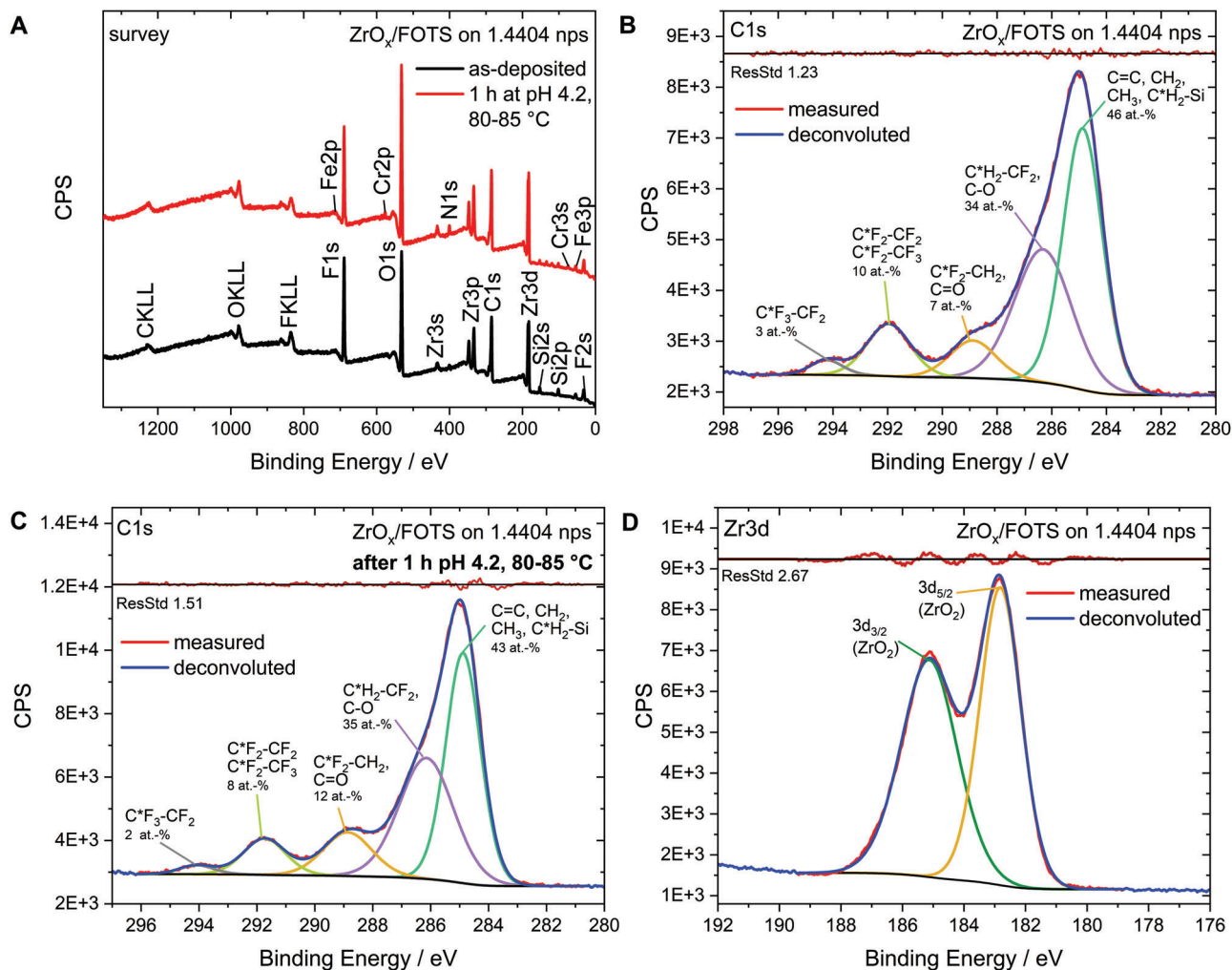**Figure 3.** Single static mixing element with the Fluitec CSE-XD6 geometry.

Figure 4. A) XPS survey and B) high-resolution core-level spectra of C1s region of thin FOTS coated 1.4404 nps surface directly after CVD process and C) after 1 h immersion into electrolyte solution at 80–85 °C and pH 4.2 as well as peak fitting. The concentrations in at.% of the assigned components are given as calculated from the HR-XPS spectra in the C1s peak region.

demonstrate their chemical resistance under process-related conditions, which is 80–85 °C and pH 4.2.

The concentrations in at.% of all detectable atoms were calculated based on the XPS spectra (**Figures 4** and **5**) allowing conclusions about the molecular surface composition. The values both for the FOTS and ZrO$_x$/FOTS coating as well as for the bare substrate are depicted in **Table 2** for comparison.

From the concentrations presented in Table 2, it becomes obvious that carbon builds up the largest part of the surface with values between 34 and 45 at.% dependent on the surface coating as expected from FOTS as a film-forming compound.

The higher surface concentration of carbon and oxygen observed for the ZrO$_x$/FOTS coated substrate is assigned to partial adsorption of adventitious carbon and to residual ligands of the

ADVANCED
SCIENCE NEWS
www.advancedsciencenews.com

{M}acro-
olecular
Reaction Engineering
www.mre-journal.de

Figure 5. A) XPS surveys and B) high-resolution core-level spectra of C1s region of thin ZrO_x/FOTS film deposited onto 1.4404 nps surface by sol-gel method before and C) after immersion into a pH 4.2 solution at 80–85 °C with respective peak fittings and the atomic concentrations (at.%) of the assigned components as calculated from the HR-XPS spectra. The spectrum in the Zr3d region D) represents the as-deposited surface state.

Table 2. Chemical composition of 1.4404 nps as well as FOTS and ZrO_x/FOTS modified substrates before and after immersion at pH 4.2 and 80–85 °C based on XPS analysis. All values are given in at.% as calculated from XPS spectra.

Stainless steel (1.4404)	C1s	O1s	F1s	Si2p	Zr3p	Fe2p	Cr2p	Ni2p	N1s
Bare substrate	40.2	41.9	–	<1	–	13.4	3.1	<1	1.2
+ FOTS coating as-deposited	34.3	7.2	53.2	5.3	–	<1	< 1	<1	<1
1 h pH 4.2, 80 °C	33.9	7.8	53.0	5.2	–	<1	< 1	<1	<1
+ ZrO_x/FOTS coating as-deposited	44.5	28.5	17.0	4.1	3.7	<1	< 1	<1	1.2
1 h pH 4.2, 80 °C	44.4	33.8	13.4	1.8	3.8	<1	< 1	<1	1.8

used zirconium precursor. The varying amount of detected fluorine can be explained by using different FOTS concentrations during film preparation. The XPS spectra further show a small amount of nitrogen, which is present on all analyzed surfaces in a similar amount and can be assigned to adventitious surface contamination. Based on the XPS probing depth[54] and the used

take-off angle of 30° the minor characteristic signals of the underlying 1.4404 nps substrate, namely for Fe2p ($\approx$ 710 eV) and Cr2p ($\approx$ 575 eV), indicate a FOTS layer thickness in the low nanometer range. This assumption is supported by performed ellipsometry measurements of FOTS deposited onto 1.4404 ps substrates and conventional silicon wafers (Siegert Wafer, see Supporting

**ADVANCED
SCIENCE NEWS**

www.advancedsciencenews.com

Macro-
molecular
Reaction Engineering

www.mre-journal.de

Information Section 2 for details), which revealed layer thicknesses of 3.8 ± 0.2 nm and 4.0 ± 0.1 nm, respectively. The observed film thickness is in good agreement with literature for FOTS deposited onto SiO_2.[37] Likewise, the sol-gel film thickness on the 1.4404 ps substrate was determined to be 5.1 ± 0.1 nm.

As evident from similar percentage areas before and after the treatment at low pH and elevated temperature, both applied surface films are assumed to be stable under process-like conditions. The Fe:Cr:Ni ratio of the bare 1.4404 nps substrate was determined to be 11:4.7:1.

To underpin the observations and to receive further information on the chemical surface structure, XPS survey and high-resolution (HR) core-level spectra of the modified surfaces at the two different surface states were analyzed in detail.

Figure 4 shows survey spectra, recorded in the 1350–0 eV range as well as core-level spectra in the C1s region of a FOTS modified 1.4404 nps surface directly after CVDdeposition as well as after a 60 min process-related exposure for comparison. The peak assignment in the deconvoluted C1s was possible due to characteristic shifts of the components based on distinct chemical environments.

As evident from Table 2, the presented survey spectra are similar for both analyzed surface states with expected photoelectron signals for carbon, oxygen, fluorine, and silicon (Figure 4A). The shown C1s core-level spectra exhibit the characteristic shape of a perfluorinated surface both before and after immersion at acidic pH and elevated temperature.[37,38,49,55] The deconvolution divides the recorded spectra into seven main peaks, six of which can clearly be assigned to the organosilan surface modification (Figure 4B,C) with some minor adventitious carbon. As can be seen from the STDRes values, good fits to the C1s envelopes are achieved. The components centered at 284.8–285.0 eV and 285.9–286.0 eV correspond to mainly C^*H_2-Si and C^*H_2-CF_2, respectively, with little CH_2, CH_3, and C–O atmospheric contributions as depicted in Figure 4B,C. Due to the fluorine environment, the C^*F_2-CH_2, CF_2-CF_2, and C^*F_2-CF_3 components are shifted to higher binding energies namely 290.7–290.8 eV, 291.4–291.5 eV, and 292.0–292.1 eV, respectively, while the CF_3 functional group gives rise to a peak at 293.6 eV. The broad peak centered at 288.2 eV or 288.6 eV, respectively, is attributed to some adventituous carbonyl and carboxyl as surface contamination.[56] Further, the percentage area ratio of all appearing components within the resolved C1s spectra were calculated and depicted in the spectra (Figure 4B,C).

The presented atomic concentrations are in good agreement with the expected theoretical values according to the perfluorinated surface depicted in Figure 1 and FOTS stoichiometry. However, it is known from the literature[55] that the CF_2:CF_3 area ratio from fits is generally below the expected theoretical value.

The (similar) values confirm both the presence of a perfluorinated film on stainless steel and the integrity of the surface even after exposure to an aqueous solution under acidic pH and elevated temperature.

Complementary XPS measurements were carried out of the ZrO_x/FOTSmodified 1.4404 nps substrates. Survey and HR-spectra in the C1s region of the as-deposited surface state and after immersion into an aqueous solution under process-like conditions are presented in Figure 5 together with the HR-core-level spectrum recorded in the Zr3d region.

Table 3. Water repellency of the pure, CVD and dip-coated 1.4404 stainless steel surfaces, respectively.

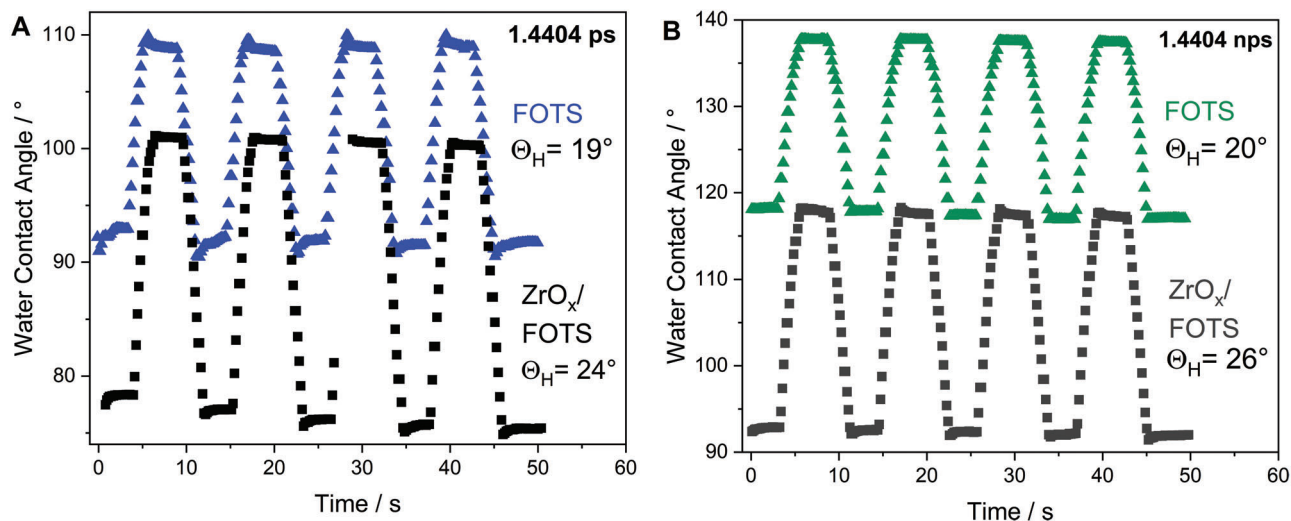| Substrate	Applied coating	Water contact angle/°
Non-polished stainless steel (nps)	–	81 ± 3.8
	FOTS	128 ± 3.1
	ZrO_x/FOTS	117 ± 2.4
Polished stainless steel (ps)	–	73 ± 2.1
	FOTS	107 ± 3.9
	ZrO_x/FOTS	104 ± 1.3

Both, before and after immersion in the electrolyte solution at pH 4.2 and 80–85 °C, the shown XPS survey spectra of the ZrO_x/FOTS films exhibit peaks assigned to carbon, oxygen, fluorine, and silicon in a similar magnitude, which suggests film stability under process-like conditions (Figure 5A). This is further supported by a deconvolution performed in the C1s peak region for both surface states, where similar atomic percentage values were derived (Figure 5B,C). Like for the FOTS coating in Figure 4B, both the C^*F_3-CF_2 and C^*F_2-CF_3/CF_2-CF_2 components could clearly be distinguished from the rest due to its characteristic chemical shift to higher binding energies. The signal at 288.9 eV is presumably an overlap of the C^*F_2-CH_2 component and the carbonyl group (C=O), which is present because of $Zr(acac)_4$ as a precursor. Likewise, the main component centered at 284.9 eV is composed of C=C contributions from the organometallic compound, C^*H_2-Si from the FOTS molecule, and CH_2/CH_3 from the atmosphere. The component at 286.3 eV could be assignable to the C^*H_2–CF_2 and adsorbates such as C–O. Additional signals attributed to the zirconium species were observed at 433 eV (Zr 3s), 331 eV (Zr 3p), and 180 eV (Zr 3d) in the survey spectra (Figure 5A). The Zr $3d_{5/2}$ and Zr $3d_{3/2}$ spin-orbit split components were detected at 182.8 eV and 185.2 eV. These peak positions indicate zirconium to be present in its fully oxidized Zr^{4+}-state[57] (Figure 5D).

3.1.2. Water Contact Angles and Wetting

The surface hydrophobicity was analyzed by performing water contact angle (WCA) measurements of the pure surface states and after the FOTS and ZrO_x/FOTS coating, respectively. The results are presented in **Table 3** for both employed types of 1.4404 stainless steel substrates.

Both the 1.4404 ps and nps substrates exhibit hydrophilic characteristics (water contact angle <90°) at the pure surface state but became clearly hydrophobic after application of the FOTS containing films. Both films applied to the 1.4404 ps substrate show almost identical water contact angles with regard of the stated errors. In contrast, the measured contact angle is reduced by 11° for the hybrid coating deposited onto the 1.4404 nps substrate in comparison to the FOTS film by CVD, which could be a result of the lowering of the surface roughness by the application of the sol-gel films. This is supported by FE-SEM images (Figure 8). It is further noticeable that the water contact angle shows consistently smaller values for the ZrO_x/FOTS than for the pure FOTS coating independent of surface roughness. The lower fluorine surface concentrations in the ZrO_x/FOTS film, as measured

Figure 6. Dynamic water contact angle of FOTS and ZrO$_x$/FOTS coated polished A) and 1.4404 nps substrates B) with contact angle hysteresis for all coatings.

by means of XPS (see Table 2), and different molecular orientations of the F-species could provide an explanation.[38]

Dynamic water contact angle measurements were performed to investigate possible changes in the wettability due to potential inhomogeneities of the surface (**Figure 6**). Subtraction of the receding contact angle (θ_r) from the advancing contact angle (θ_a) provides information about the contact angle hysteresis (θ_H), the origin of which is detailly discussed by Eral et al.[58]

The water contact hysteresis observed for the FOTS and ZrO$_x$/FOTS coating exhibit values between 19 and 26° on both examined stainless steel surfaces, which is in a typical range for hydrophobic coatings such as fluorosilanes[59] or poly(tetrafluoroethylene) (PTFE).[60] On both surfaces, the hysteresis for the CVD coating is smaller than for the hybrid-coating, which is in accordance with the previously discussed (static) water contact angles and the statements regarding roughness and surface inhomogeneities.

By measuring the contact angles on thin films coated 1.4404 ps substrates with liquids of varying polar and dispersive components, the total SFE was calculated to be 14.6 mN m^{-1} (γd: 11.8 mN m^{-1}, γp: 2.8 mN m^{-1}) for the FOTS and 20.3 mN m^{-1} (γd: 18.9 mN m^{-1}, γp: 1.4 mN m^{-1}) for the ZrO$_x$/FOTS coating. This is significantly lower than the SFE of the used 1.4404 ps surface, which was experimentally determined to be 41 mN m^{-1}. The value lies in the expected range for polished stainless steel.[61] It is slightly lower than the SFE reported for PTFE[61,62] and in the range of other fluorine-incorporated organosilicon[63] or hydrophobic copolymer coatings.[38] However, it is not as low as 6 mN m^{-1}, which is the lowest SFE reported in the literature for a surface carrying a uniformly organized crystalline array of CF$_3$-groups.[33] This suggests a less ordered structure of the F-moiety on the solid surfaces in this study.
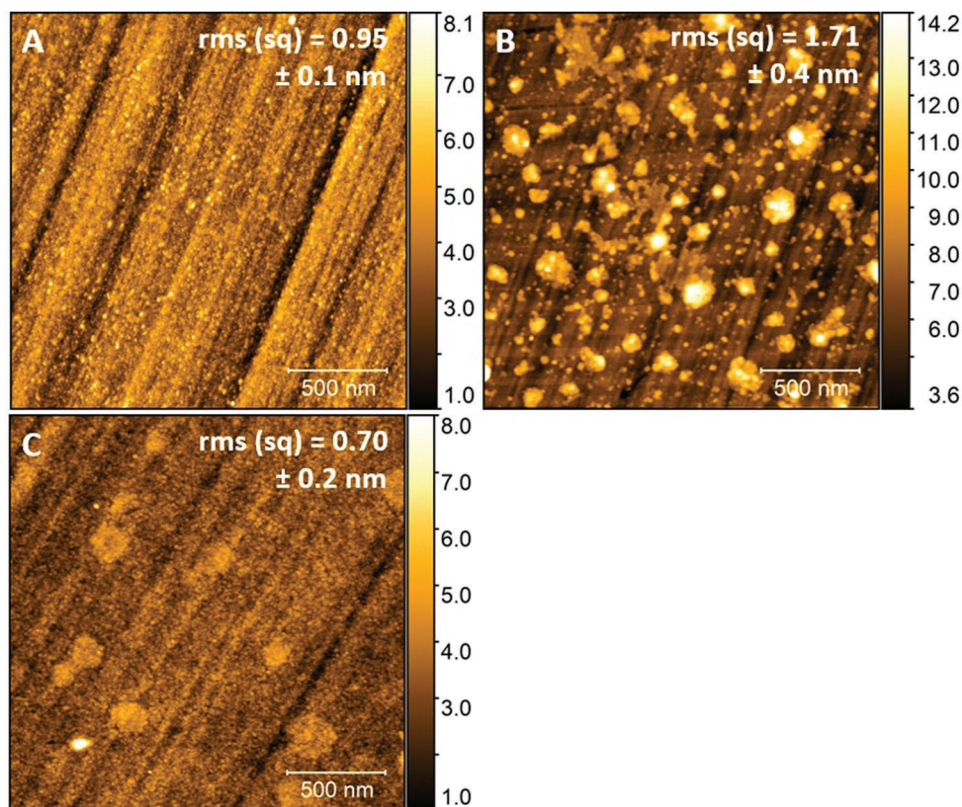
3.1.3. Surface Morphology of Thin Films

The surface morphology was analyzed by employing FE-SEM and AFM imaging. High-resolution AFM images of the 1.4404 ps

substrate before and after modification with the FOTS and ZrO$_x$/FOTS coating are shown in **Figure 7**. Roughness parameters, such as the root-mean-square roughness (rms(sq)) values were calculated to characterize the surface topography.

The AFM image of the FOTS coated 1.4404 ps surface (Figure 7B) implies a defect-containing multilayer film with islands up to a height of $\approx$ 14 nm. The presence of smaller surface defects was proven by cyclic voltammograms. Further details are given in the Supporting Information, Section 3, Figure S3B. The island-like film structure leads to an increase of the surface roughness from $\approx$ 1.0 nm on the bare substrate to about 1.7 nm on the FOTS modified surface. In contrast, the surface roughness of the substrate after applying the ZrO$_x$/FOTS film (Figure 7C) is slightly lower than on the bare surface, as evident from the rms(sq) value of 0.7 nm. Even though small island-like formed structures could be detected, the surface is homogeneously covered by the film. Full surface coverage could be confirmed by cyclic voltammetry (Supporting Information, Section 3, Figure S3C). It can further be concluded that the depth of the grooves and minor surface irregularities, obvious from Figure 7A, are reduced. This is supported by FE-SEM images, recorded of the bare 1.4404 nps surface as well as after the deposition of the ZrO$_x$/FOTS hybrid film, which are shown in **Figure 8**.

From the FE-SEM image shown in Figure 8A it is obvious that the topography of the employed 1.4404 nps substrate exhibits a structure with trenches of a depth of $\approx$300 nm up to $\approx$1.6 μm (Figure 8C). In addition, small troughs could be observed on the plateaus, which further increase the roughness (Figure 8A, top left, and right). From the images shown in Figure 8B,D it is evident that the ZrO$_x$/FOTS film fills these indentations. Less amount of the film is deposited on top of the surface, as confirmed by Electron Dispersive X-ray analysis (EDX)-measurements (Figure S4 and Table S1, Supporting Information). This leads to a partial smoothening and a decreased surface roughness, which confirms the observation made from AFM-images and is both characteristic and one advantage of a coating applied by the sol-gel method.[43]

**ADVANCED
SCIENCE NEWS**

www.advancedsciencenews.com

[M] acro-
olecular
Reaction Engineering

www.mre-journal.de

Figure 7. A) (2×2) μm^2 AFM images of bare 1.4404 ps substrate, B) the latter after FOTS deposition by CVD and C) after ZrO_x/FOTS coating applied by sol-gel method. The rms-value given is the root-mean-square roughness of the respective surface with standard deviation.

4. Performance of Thin Film Coated Microreactor Components

In the following, the results of the fouling experiments performed in the microreactor (see Section 2.4 for details), are presented for the previously described uncoated and FOTS as well as ZrO_x/FOTS coated mixing elements. To analyze changes in surface properties after exposition to reaction conditions, flat uncoated and coated 1.4404 nps plates were placed into the microreactor outlet for each experiment. These plates were subsequently analyzed by FTIR spectroscopy.

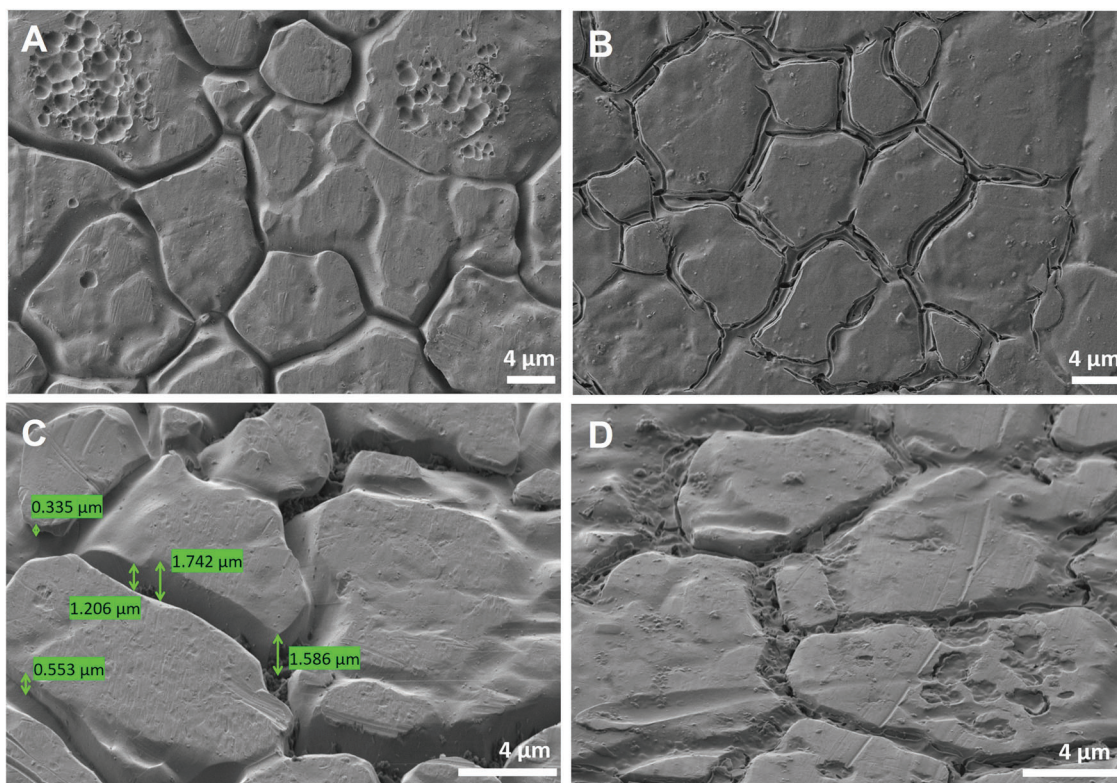### 4.1. Evolution of Pressure Drop During Operation Time

Figure 9 shows a comparison of the pressure drop evolution during operation time using coated and uncoated mixer elements. After the startup of the polymerization the pressure drop increases in all experiments due to an increase of viscosity (first 30 min). Then the pressure stays constant for roughly 8 h in all cases. The small recurring peaks in the pressure signal are due to sampling extraction from the reactor. The measured monomer conversion is in the range of 7%–15%. No significant differences in the conversion rate were found between uncoated and coated mixers.

Uncoated mixers: After eight hours of operation, the pressure drop starts to increase for the uncoated stainless steel mixing elements and becomes more and more volatile (Figure 9). This can

be attributed to the accumulation of an insoluble polymer gel, which adheres to the casted steel mixer elements and blocks the free volume in the reactor. The pressure increases continuously until the end of the experiment, where the absolute pressure loss is ≈150 mbar compared to the reactor inlet. Then the reactor is rinsed with water (Figure 9, grayed area). Part of the clogging is removed by water flushing, however, the pressure does not return to the initial value. This indicates persistent adherence of gel on the uncoated mixers.

FOTS coated mixers: The operation of the reactor over 10 h using FOTS coated mixers does not lead to an increase of pressure drop (Figure 9). Thus, employing FOTS coated mixing elements leads to a significant increase of operation time in the radical polymerization of PVP. Small fluctuations in the pressure profile (for instance after 4 h) may be due to locally increased viscosity in the outlet of the reactor, which is an uncoated stainless steel element. After the end of the polymerization experiment, the reactor is rinsed with water. Contrary to the uncoated mixers, the pressure signal returns to the initial state (Figure 9, colored gray). This clearly indicates, that either no gel deposits are formed, or they are weakly bound to the surface and can be removed easily.
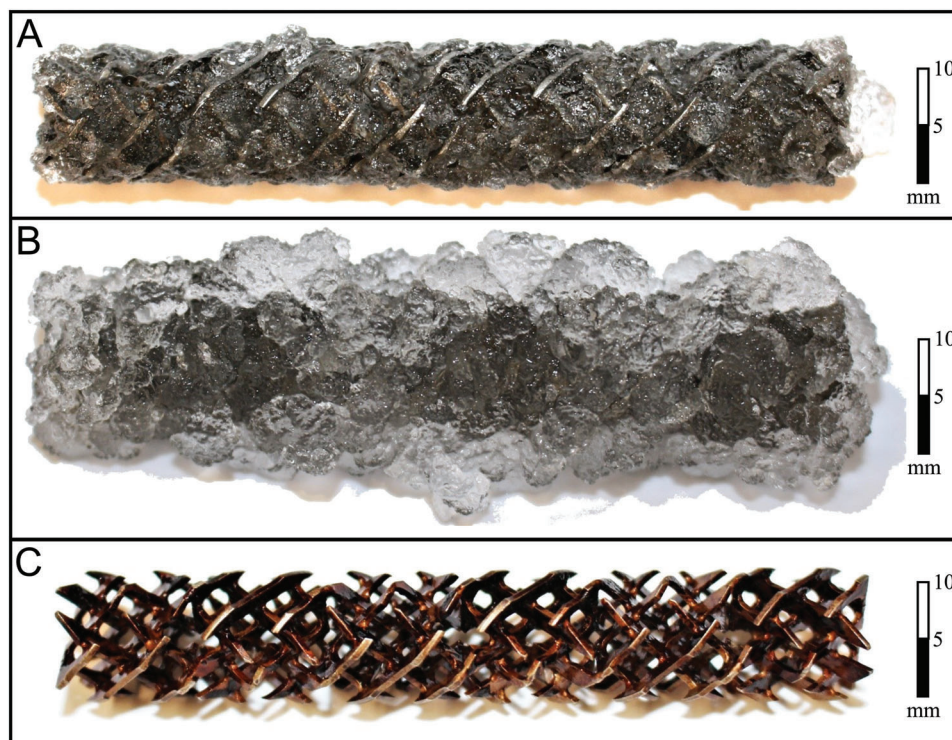
ZrO_x/FOTS coated mixers: The second hydrophobic coating is the ZrO_x/FOTS coating on factory fresh stainless steel mixing elements. Figure 9 shows the pressure drop for the coated mixing elements. The pressure profile increases initially due to viscosity changes and then stays constant. After flushing with water (Figure 9, colored gray), the initial pressure is reached again.

**ADVANCED
SCIENCE NEWS**

www.advancedsciencenews.com

M acro-
molecular
Reaction Engineering

www.mre-journal.de

Figure 8. A) FE-SEM images of solvent cleaned 1.4404 nps surface with 2500 x magnification and B) the comparable surface after applying the ZrO_x/FOTS film by sol-gel method as well as C) the bare substrate with 5000 x magnification with 36° tilt and D) the latter after application of the ZrO_x/FOTS film. The hydrophobic coating fills up surface rifts which could further be confirmed by Electron Dispersive X-ray (EDX) analysis as presented in Figure S4 and Table S1, Supporting Information.
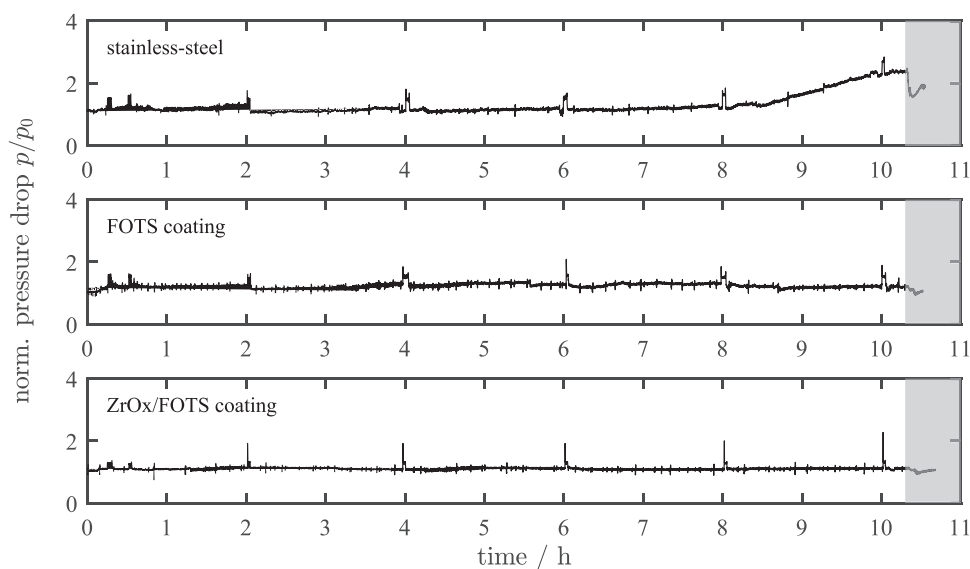
Figure 9. Comparison of the normalized entry pressure evolution in experiments with and without the hydrophobic coating. The experiments have been conducted as described in Section 2.4 and Table 1 with a superficial velocity of 5 mm s^{-1}. $p_0 = p(0 \text{ h})$.

**ADVANCED
SCIENCE NEWS**

www.advancedsciencenews.com

**[M]acro-molecular
Reaction Engineering**

www.mre-journal.de

Figure 10. A) PVP gel fouling on a casted steel static mixer element and B) swollen PVP gel on a casted steel static mixer element as well as C) a water jet cleaned uncoated mixing element, which was additionally placed in an iodine-water solution. The experiment has been conducted as described in Section 2.4 and Table 1 with a superficial velocity of 5 mm s^{-1}.

Compared to uncoated mixing elements, the operation time can be significantly increased.

4.2. Gel Formation on Dismounted Mixing Elements

After completion of the experiments, the mixing elements are dismounted. In order to visualize the residual gel, the dismounted mixing elements are placed in deionized water overnight. In the second step, the mixers are cleaned with a water jet until all visible polymer is removed. Then they are placed in a 0.1 N iodine-water solution for 5 min, which allows to detect of residual gel deposition on the surface. The PVP-Iodine complex formation (Supporting Information, Figure S5) results in a red-brown coloration of the polymer.[64–66]

Uncoated mixers: An uncoated mixer element is shown in **Figure 10**A. The polymer gel has accumulated and blocked most of the free volume in the reactor.

By placing the dismounted mixer elements in deionized water overnight, the accumulated gel could be swollen. The result is a mixer, shown in Figure 10B, which is no longer visible due to the swollen gel.

While only small amounts of polymer gel accumulated at the beginning of the run with factory-fresh mixer elements, the amounts increased to the state that is shown in Figure 10A over time.

While in the entrance region of the reactor only a small amount of fouling occurs, the amount increases along the reactor length.

This insight can be explained by the initial heating distance in the reactor.

After the experiment, the mixer elements are cleaned with a water jet. Figure 10C shows the uncoated mixing element after the cleaning procedure and exposition to the iodine-water solution. Even after cleaning with a water jet the whole surface of the mixing element is coated with a PVP layer.

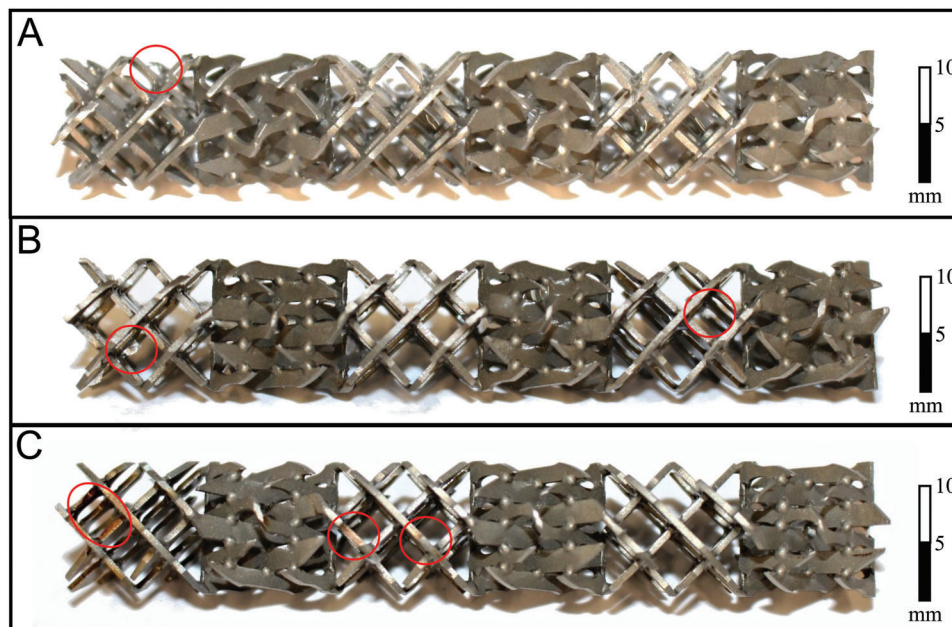### 4.3. Initial State with Applied Thin Films

Since the adhesion of macromolecules seems to be an important part of the fouling mechanism, experiments with different surface modifications have been carried out.

FOTS coated mixers: A mixer element from the experiment described above is shown in **Figure 11**A. Minor fouling can be observed in regions close to the metal reactor walls. These fouling deposits could easily be removed by rinsing with water.

By placing the dismounted mixer elements in water overnight, the accumulated gel becomes visible. Figure 11B shows that only small amounts of swollen PVP gel are attached on the coated mixing element.

Figure 11C shows the FOTS coated static mixer element after the cleaning procedure and complexing reaction with iodine. Clearly, on the most part of the surface, no PVP can be seen.

It can therefore be concluded that a FOTS coated surface not only significantly reduces the amount of fouling, but also enhances the cleaning process drastically.

**ADVANCED
SCIENCE NEWS**

www.advancedsciencenews.com

{M} acro-
olecular
Reaction Engineering

www.mre-journal.de

Figure 11. A) Minor fouling due to hydrophobic coatings (FOTS) on casted steel static mixer element and B) small amounts of swollen PVP gel on hydrophobic coatings (FOTS) on casted steel static mixer element as well as C) the water jet cleaned coated (FOTS) mixing element, which was additionally placed in an iodine-water solution. The experiment has been conducted as described in Section 2.4 and Table 1 with a superficial velocity of 5 mm s^{-1}.
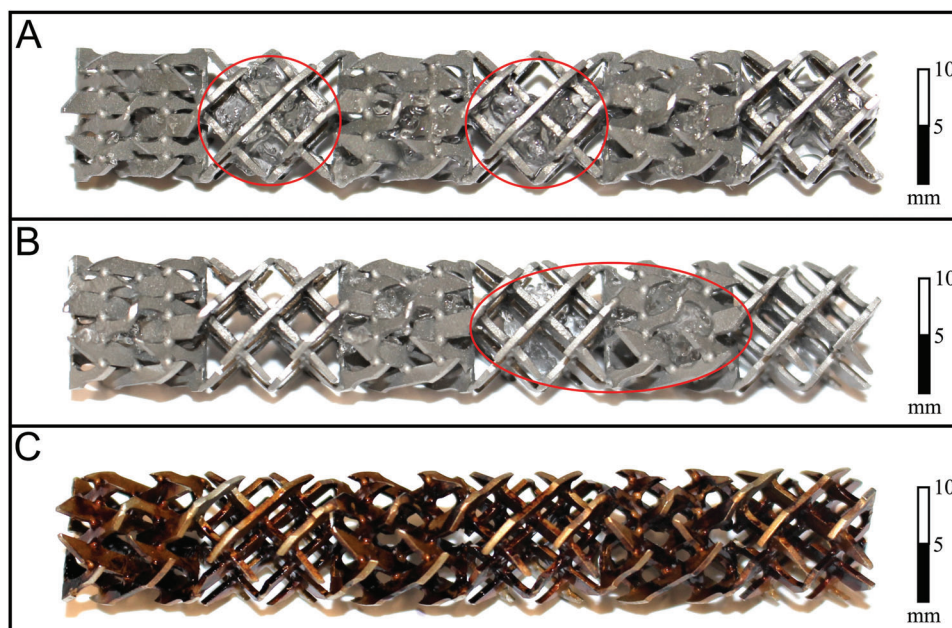
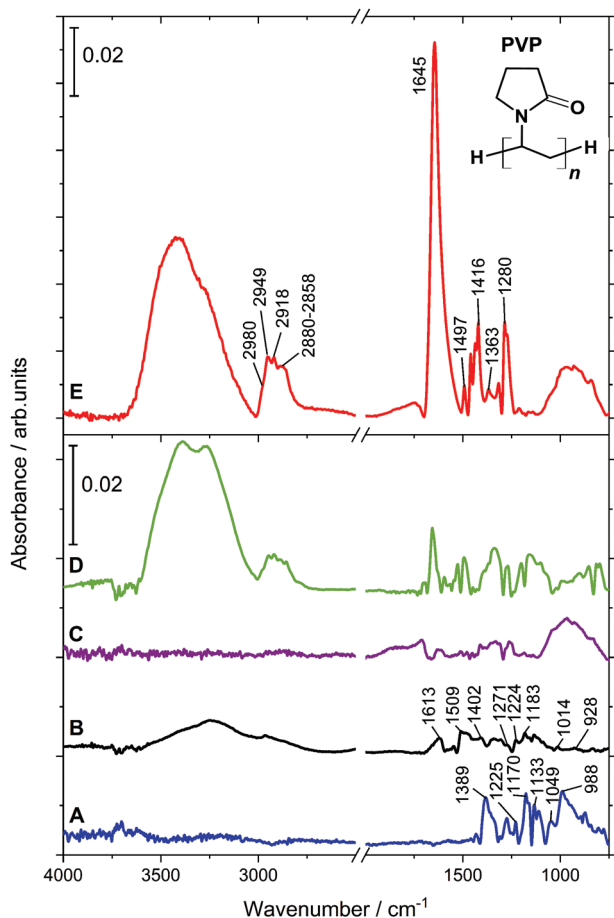**Figure 12.** A) Minor fouling due to hydrophobic coatings (ZrO$_x$/FOTS) on casted steel static mixer element and B) small amounts of swollen PVP gel on hydrophobic coatings (ZrO$_x$/FOTS) on casted steel static mixer element as well as C) the water jet cleaned coated (ZrO$_x$/FOTS) mixing element, which was additionally placed in an iodine-water solution. The experiment has been conducted as described in Section 2.4 and Table 1 with a superficial velocity of 5 mm s^{-1}.

ZrO$_x$/FOTS coated mixers: **Figure 12**A shows the coated mixing element after the operation time with a small amount of gel deposits.

The mixer elements are again dismounted and placed in water overnight to make accumulated gel better visible. Figure 12B

shows that only small amounts of swollen PVP gel have been attached on the coated mixing element.

Figure 12C shows the ZrO$_x$/FOTS coated mixing element after the cleaning procedure and complexing reaction with iodine. It is clearly visible that the surface is colored brown-red by iodine,

**ADVANCED
SCIENCE NEWS**

www.advancedsciencenews.com

**[M]acro-
olecular
Reaction Engineering**

www.mre-journal.de

Figure 13. A) FTIR spectra of the as-prepared FOTS and B) ZrO_x/FOTS film coated 1.4404 nps surface as well as C) FOTS and D) ZrO_x/FOTS modified substrate after contact with PVP in the microreactor for one reaction cycle and subsequent water cleaning process in comparison to E) analogously treated bare nps surface. A solvent cleaned nps substrate served as reference.

so PVP deposits on the surface of the mixing element are clearly visible. Nevertheless, it should be mentioned that much less gel forms on the mixers due to the coating compared to the uncoated mixers.

In the Supporting Information, a blank sample (ZrO_x/FOTS on a 1.4404 nps plate) is shown after iodine treatment (Figure S6, Supporting Information) to exclude a possible complexation reaction of iodine with the ZrO_x complex.

4.3.1. Post FTIR-Analysis of In-Process Prepared Samples

In order to further analyze the microscopic effectiveness of the described FOTS and ZrO_x/FOTS films, bare and modified 1.4404 nps substrates with flat geometry were placed at the reactor outlet during one reaction cycle, followed by a 24 h water bath treatment. Afterward, FTIR spectra were recorded. The obtained spectra are shown in **Figure 13**, along with spectra recorded of the bare 1.4404 nps substrate after contact with a polymer solution and a subsequent water bath treatment and the as-prepared FOTS and

ZrO_x/FOTS hybrid films. In all cases, a solvent-cleaned 1.4404 nps substrate served as a reference.

The FOTS modified substrate shows characteristic IR-signals for a FOTS film (Figure 13A). The CH-deformation modes from CH_2-groups produce a conspicuous band at 1389 cm^{-1},[67] while the peaks located at 1225 cm^{-1} and 1170 cm^{-1} correspond to the asymmetric and symmetric stretching frequency of the CF_2-groups,[68,69] respectively. The peak at 1133 cm^{-1} can be assigned to Si—O—C bonds.[70] The signal at 1049 cm^{-1} can be attributed to the characteristic siloxane bonds (v_a Si—O—Si)[70,71] and the Si–OH bending gives rise to a well-developed peak ≈988 cm^{-1}.[72] In addition to the OH-band of adsorbed water, which can be distinguished into "liquid" (≈3400 cm^{-1}) and "ice-like" (≈3200 cm^{-1}),[73] another weak band was detected in the spectrum at wavenumbers >3600 cm^{-1}. This band can be attributed to isolated or terminal silanol groups.[73] It was previously observed on FOTS modified surfaces and could be explained by the possibility of water adsorption into nanoscopic surface defects.[74]

Even though the absolute structure of the hybrid film is not completely clarified in this study, the major bands appearing in the FTIR spectrum of the ZrO_x/FOTS coated 1.4404 nps substrate can be identified (Figure 13B). A distinctive OH-absorption band appears above 3000 cm^{-1},[75] while the band below 3000 cm^{-1} can be related to CH-stretching of CH_n-groups present in both the FOTS molecule and metal-organic precursor with corresponding CH-deformation vibrations at 1402 cm^{-1}. Another characteristic peak at 1613 cm^{-1} can be attributed to a CO-stretching vibration of the Zr(acac)$_4$ complex[76] with a shoulder appearing at higher wavenumbers, which suggests an overlap with δ(HOH)-bending vibrations of water molecules in the mentioned region.[76,77] The C–C-stretching vibrations produce peaks at 1509 cm^{-1} and 1271 cm^{-1} with the latter probably being affected by contributions from Si-CH$_2$ vibrations from the FOTS.[72] While the presence of CF_2– and CF_3-groups is confirmed by a signal at 1224 cm^{-1},[70] peaks located at 1183 cm^{-1}, 1014 cm^{-1}, and 928 cm^{-1} can most probably be attributed to a combination of bending δ(CCH) with C–C-stretching, originating from the ligands of the Zr-complex.[76] Bands corresponding to the stretching of Zr-O$_{acac}$ or Zr–F should appear at wavenumbers below 500 cm^{-1},[76,78] but were not observed in this study due to the use of a mid-infrared IR-spectrometer.

In the case of the unmodified stainless steel substrate after contact with the polymeric media (Figure 13E), the FTIR spectrum exhibits distinctive stretching bands at 1645 cm^{-1} and 1416 cm^{-1} corresponding to the pyrrolidone C=O group as well as hydrocarbon absorption of PVP.[67] Two bands located at 1280 cm^{-1} and 1497 cm^{-1} can be ascribed to the C–N-stretching.[79] In addition, the CH_2-stretching vibrations of the pyrrole ring and chain produce well-defined local peak maxima at 2949 cm^{-1} and 2980 cm^{-1} (asymmetric) as well as 2880 cm^{-1} and 2918 cm^{-1} (symmetric). In this region, another minor maximum is located at 2858 cm^{-1} corresponding to ternary CH-stretching vibrations.[67,80] Overall, the mentioned peaks clearly confirm the presence of PVP on the substrate. Further, the strong absorption band at wavenumbers above 3400 cm^{-1} corresponds to the OH-stretching of adsorbed water which indicates hydrogel formation.

In contrast to this, the PVP characteristic bands are only slightly developed on the FOTS modified surface after contact

**ADVANCED
SCIENCE NEWS**

www.advancedsciencenews.com

Macro-
molecular
Reaction Engineering

www.mre-journal.de

with the polymer (Figure 13C), which underlines the strong anti-fouling properties of the thin film.

The ZrO$_x$/FOTS coated 1.4404 nps substrate after contact with the polymeric media (Figure 13D) shows marginally PVP-characteristic signals in comparison to the uncoated nps reference substrate (Figure 13E). Although the peaks corresponding to the CH$_2$-stretching vibrations of the pyrrole ring and chain (2800–3000 cm^{-1}) can still be assigned, especially the distinctive band of the C=O-group is clearly reduced, which supports the previously shown results regarding anti-adhesive properties of the hybrid film.

5. Conclusions

Coatings with the aim of deposit-reducing effects are widely discussed in the literature for various systems where fouling occurs.[8,14,19,25,45] However, regarding the desired anti-fouling effect in microreactors for polymerization processes the preservation of microstructures through the application of ultra-thin films is decisive.

Within this study, two films with low surface free energy and nanometer-scale thickness, namely a FOTS and a FOTS-containing zirconium oxide sol-gel film on 1.4404 stainless steel substrates, were comparatively investigated.

FOTS CVD films with an average thickness of 3.8 nm showed a rather island like-structure however, led to a very low surface energy of 14.6 mN m^{-1}. In comparison, the sol-gel deposited ZrO$_x$/FOTS films were quite smooth even at a film thickness of 5.1 nm. Based on the lower concentration of FOTS in the surface near region as measured by XPS, the ZrO$_x$/FOTS films showed a slightly higher surface energy. However, the sol-gel application even led to a smoothening of rough technical substrates. XPS data proved the stability of the applied films under process-relevant conditions.

The analysis of static stainless steel mixing elements employed during the radical polymerization of NVP to PVP in an aqueous solution in real microreactors allowed us to visually and, by recording pressure profiles, also physically detect the widely discussed phenomenon of fouling,[2,3,12] caused by polymers in (micro)reactors. By application of the coatings to the static mixing elements, the amount of polymeric deposit could significantly be reduced. In this regard, the low polar components determined for both coatings are presumably responsible for reduced interactions appearing at the solid/liquid interface. On the one hand, the FOTS applied by CVD in particular showed outstanding anti-adhesive properties with almost no PVP-deposit formation, as further demonstrated by FTIR analysis. On the other hand, the ZrO$_x$/FOTS film led to the desired reduction of the surface roughness and an improved lateral surface homogeneity. In addition, the sol-gel film showed higher barrier properties than the FOTS-CVD films.

Even though long-time experiments are still pending, both films allow the microreactor for the polymerization process to be used for longer periods without the need for time and cost-consuming rinsing steps in between. Due to their low surface energy and the chemical inertness of the deposited films the presented strategy could be transferred to other water-soluble polymer systems synthesized in a similar process.

Conflict of Interest

The authors declare no conflict of interest.

Author Contributions

V.N. and S.W. contributed equally to this work. V.N.: Data Curation, Formal analysis, Investigation, Methodology, Visualization, Conceptualization, Validation, Writing – Original Draft. S.W.: Data Curation, Formal analysis, Investigation, Methodology, Visualization, Validation, Writing – Original Draft. F.R.: Methodology. D. M.: Conceptualization, Supervision, Writing – Review & Editing. U.N.: Funding acquisition, Project administration, Resources, Supervision, Writing – Review & Editing. G.G.: Conceptualization, Funding acquisition, Project administration, Resources, Supervision, Writing – Review & Editing.

Data Availability Statement

The data that support the findings of this study are available from the corresponding author upon reasonable request.

[1] D. Kohlmann, M.-C. Chevrel, S. Hoppe, D. Meimaroglou, D. Chapron, P. Bourson, C. Schwede, W. Loth, A. Stammer, J. Wilson, P. Ferlin, L. Falk, S. Engell, A. Durand, *Macromol. React. Eng.* **2016**, *10*, 339.

[2] C. N. Zander, Doctoral Thesis, Fouling during solution polymerization in continuously operated reactors, University of Stuttgart **2021**.

[3] M. F. Cunningham, K. F. O'driscoll, H. K. Mahabadi, *Polym. React. Eng.* **1993**, *1*, 245.

[4] W. Guo, H.-H. Ngo, J. Li, *Bioresour. Technol.* **2012**, *122*, 27.

[5] J.- M. Laãñã©, C. Campos, I. Baudin, M.- L. Janex, *Water Supply* **2003**, *3*, 155.

[6] X. Zhang, D. Brodus, V. Hollimon, H. Hu, *Chem. Cent. J.* **2017**, *11*, 18.

[7] S. Zouaghi, T. Six, N. Nuns, P. Simon, S. Bellayer, S. Moradi, S. G. Hatzikiriakos, C. André, G. Delaplace, M. Jimenez, *J. Food Eng.* **2018**, *228*, 38.

[8] R. Rosmaninho, O. Santos, T. Nylander, M. Paulsson, M. Beuf, T. Benezech, S. Yiantsios, N. Andritsos, A. Karabelas, G. Rizzo, H. Müller-Steinhagen, L. F. Melo, *J. Food Eng.* **2007**, *80*, 1176.

[9] E. Sadeghinezhad, S. N. Kazi, A. Badarudin, M. N. M. Zubair, B. L. Dehkordi, C. S. Oon, *Rev. Chem. Eng.* **2013**, *29*.

[10] L. M. Al-Harbi, S. A. Kosa, M. K. Baloch, Q. A. Bhatti, E.l-S. E.l-B. H. El-Mossalamy, *Int. J. Polym. Sci.* **2016**, *2016*, 2417292.

[11] C. Zander, K.-D. Hungenberg, T. Schall, C. Schwede, U. Nieken, *Macromol. React. Eng.* **2020**, *14*, 2000009.

[12] P. Deglmann, M. Hellmund, K.-D. Hungenberg, U. Nieken, C. Schwede, C. Zander, *Macromol. React. Eng.* **2019**, *13*, 1900021.

[13] S. Welzel, C. Zander, K.- D. Hungenberg, U. Nieken, *Macromol. React. Eng.* **2022**, *16*, 2200005.

[14] A. Pistone, C. Scolaro, A. Visco, *Polymers* **2021**, *13*, 173.

[15] Y. Higaki, M. Kobayashi, D. Murakami, A. Takahara, *Polym. J.* **2016**, *48*, 325.

[16] F. Wang, H. Zhang, B. Yu, S. Wang, Y. Shen, H. Cong, *Prog. Org. Coat.* **2020**, *147*, 105860.

[17] J. H. Jhaveri, Z. V. P. Murthy, *Desalination* **2016**, *379*, 137.

[18] M. R. Malayeri, A. Al-Janabi, H. Müller-Steinhagen, *Int. J. Energy Res.* **2009**, *33*, 1101.

[19] V. Oldani, C. L. Bianchi, S. Biella, C. Pirola, G. Cattaneo, *Heat Transfer Eng.* **2016**, *37*, 210.

[20] K. Bobzin, R. Nickel, N. Bagcivan, F. D. Manz, *Plasma Process. Polym.* **2007**, *4*, S144.

[21] K. Bobzin, N. Bagcivan, A. Gillner, C. Hartmann, J. Holtkamp, W. Michaeli, F. Klaiber, M. Schöngart, S. Theiß, *Prod. Eng. Res. Dev.* **2011**, *5*, 415.

[22] F. Silva, R. Martinho, M. Andrade, A. Baptista, R. Alexandre, R. Alexandre, *Coatings* **2017**, *7*, 28.

[23] L. Cunha, M. Andritschky, K. Pischow, Z. Wang, A. Zarychta, A. S. Miranda, A. M. Cunha, *Surf. Coat. Technol.* **2002**, *153*, 160.

[24] C. Theile-Rasche, M. Wiesing, S. Schwiderek, M. Noeske, G. Grundmeier, *Appl. Surf. Sci.* **2020**, *523*, 145701.

[25] V. Oldani, R. Del Negro, C. L. Bianchi, R. Suriano, S. Turri, C. Pirola, B. Sacchi, *J. Fluorine Chem.* **2015**, *180*, 7.

[26] T. P. Knepper, F. T. Lange, Eds., *The Handbook of Environmental Chemistry: Polyfluorinated Chemicals and Transformation Products*, Springer, Berlin **2012**.

[27] T. Frömel, T. P. Knepper, in *Polyfluorinated Chemicals and Transformation Products*, Vol. *17* (Eds.: T. P. Knepper, F. T. Lange), Springer, Berlin Heidelberg. Berlin, Heidelberg **2012**, p. 41.

[28] K. Izumi, H. Tanaka, M. Murakami, T. Deguchi, A. Morita, N. Tohge, T. Minami, *J. Non-Cryst. Solids* **1990**, *121*, 344.

[29] J. C. Calderã³N, L. Koch, C. Bandl, W. Kern, J. Jilg, C. Schilp, E. Moritzer, G. Grundmeier, *Surf. Coat. Technol.* **2020**, *399*, 126152.

[30] B. Kaynak, C.ã¼ Alpan, M. Kratzer, C. Ganser, C. Teichert, W. Kern, *Appl. Surf. Sci.* **2017**, *416*, 824.

[31] D. O'hagan, *Chem. Soc. Rev.* **2008**, *37*, 308.

[32] S. Pletincx, J. M. C. Mol, H. Terryn, A. Hubin, T. Hauffman, *J. Electroanal. Chem.* **2019**, *848*, 113311.

[33] W. A. Zisman, in *Contact Angle, Wettability, and Adhesion*, Vol. *43* (Ed.: F. M. Fowkes), American Chemical Society, Washington, DC **1964**, p. 1.

[34] H. Yano, K. Mori, K. Koshiishi, K. Masuhara, *J. Surf. Finish. Soc. Jpn.* **1989**, *40*, 110.

[35] D. F. Cheng, B. Masheder, C. Urata, A. Hozumi, *Langmuir* **2013**, *29*, 11322.

[36] J. Cech, R. Taboryski, *Appl. Surf. Sci.* **2012**, *259*, 538.

[37] A. Hozumi, K. Ushiyama, H. Sugimura, O. Takai, *Langmuir* **1999**, *15*, 7600.

[38] J. Gao, D. Yan, H. Ni, L. Wang, Y. Yang, X. Wang, *J. Colloid Interface Sci.* **2013**, *393*, 361.

[39] M. Cichomski, K. Kośla, W. Kozłowski, W. Szmaja, J. Balcerski, J. Rogowski, J. Grobelny, *Appl. Surf. Sci.* **2012**, *258*, 9849.

[40] J.- D. Brassard, D. K. Sarkar, J. Perron, *Appl. Sci.* **2012**, *2*, 453.

[41] W. Xu, H. Liu, S. Lu, J. Xi, Y. Wang, *Langmuir* **2008**, *24*, 10895.

[42] T. M. Racheva, G. W. Critchlow, *Thin Solid Films* **1997**, *292*, 299.

[43] D. R. Uhlmann, T. Suratwala, K. Davidson, J. M. Boulton, G. Teowee, *J. Non-Cryst. Solids* **1997**, *218*, 113.

[44] P. Fabbri, M. Messori, M. Montecchi, S. Nannarone, L. Pasquali, F. Pilati, C. Tonelli, M. Toselli, *Polymer* **2006**, *47*, 1055.

[45] S. Kwon, H. Kim, J.-W. Ha, S.-Y. Lee, *J. Ind. Eng. Chem.* **2011**, *17*, 259.

[46] S. Venkataraj, O. Kappertz, H. Weis, R. Drese, R. Jayavel, M. Wuttig, *J. Appl. Phys.* **2002**, *92*, 3599.

[47] S. H. Messaddeq, S. H. Pulcinelli, C. V. Santilli, A. C. Guastaldi, Y. Messaddeq, *J. Non-Cryst. Solids* **1999**, *247*, 164.

[48] M. Mantel, J. P. Wightman, *Surf. Interface Anal.* **1994**, *21*, 595.

[49] H. Sugimura, A. Hozumi, T. Kameyama, O. Takai, *Surf. Interface Anal.* **2002**, *34*, 550.

[50] D. Nečas, P. Klapetek, *Open Phys.* **2012**, *10*, 181.

[51] G. Ström, M. Fredriksson, P. Stenius, *J. Colloid Interface Sci.* **1987**, *119*, 352.

[52] J. M. Schuster, C. E. Schvezov, M. R. Rosenberger, *Procedia Mater. Sci.* **2015**, *8*, 732.

[53] D. K. Owens, R. C. Wendt, *J. Appl. Polym. Sci.* **1969**, *13*, 1741.

[54] W. Fredriksson, S. Malmgren, T. Gustafsson, M. Gorgoi, K. Edström, *Appl. Surf. Sci.* **2012**, *258*, 5790.

[55] B. I. Johnson, T. G. Avval, J. Wheeler, H. C. Anderson, A. Diwan, K. J. Stowers, D. H. Ess, M. R. Linford, *Langmuir* **2020**, *36*, 1878.

[56] D. T. Clark, D. Shuttleworth, *J. Polym. Sci.: Polym. Chem. Ed.* **1980**, *28*, 27.

[57] N. L. Zhang, Z. T. Song, Q. Wan, Q. W. Shen, C. L. Lin, *Appl. Surf. Sci.* **2002**, *202*, 126.

[58] H. B. Eral, D. J. C. M. 't Mannetje, J. M. Oh, *Colloid Polym. Sci.* **2013**, *291*, 247.

[59] J. Bico, C. Marzolin, D. Quéré, *Europhys. Lett.* **1999**, *47*, 743.

[60] O. N. Tretinnikov, Y. Ikada, *Langmuir* **1994**, *10*, 1606.

[61] C. I. Pereni, Q. Zhao, Y. Liu, E. Abel, *Colloids Surf., B* **2006**, *48*, 143.

[62] Y. Kitazaki, T. Hata, *J. Adhes.* **1972**, *4*, 123.

[63] D. N. Bender, K. Zhang, J. Wang, G. Liu, *ACS Appl. Mater. Interfaces* **2021**, *13*, 10467.

[64] R. F. Cournoyer, S. Siggia, *J. Polym. Sci.: Polym. Chem. Ed.* **1974**, *12*, 603.

[65] S. Siggia, *J. Am. Pharm. Assoc., Sci. Ed.* **1957**, *46*, 201.

[66] I. Sebe, B. Szabó, Z. K. Nagy, D. Szabó, L. Zsidai, B. Kocsis, R. Zelkó, *Int. J. Pharm.* **2013**, *458*, 99.

[67] I. A. Safo, M. Werheid, C. Dosche, M. Oezaslan, *Nanoscale Adv.* **2019**, *1*, 3095.

[68] S. J. Limb, K. K. Gleason, D. J. Edell, E. F. Gleason, *J. Vac. Sci. Technol., A* **1997**, *15*, 1814.

[69] T. Shirafuji, Y. Miyazaki, Y. Nakagami, Y. Hayashi, S. Nishino, *Jpn. J. Appl. Phys.* **1999**, *38*, 4520.

[70] T. Li, S. Zeng, Y. Ji, B. Shen, Z. Wang, H. Zhong, S. Wang, *Appl. Sci.* **2019**, *9*, 2619.

[71] V. Barranco, P. Thiemann, H. K. Yasuda, M. Stratmann, G. Grundmeier, *Appl. Surf. Sci.* **2004**, *229*, 87.

[72] Y. Cai, J. Li, L. Yi, X. Yan, J. Li, *Appl. Surf. Sci.* **2018**, *450*, 102.

[73] B. Torun, C. Kunze, C. Zhang, T. D. Kühne, G. Grundmeier, *Phys. Chem. Chem. Phys.* **2014**, *16*, 7377.

[74] I. Giner, B. Torun, Y. Han, B. Duderija, D. Meinderink, A. G.¡.L. Orive, T. De Los Arcos, C. Weinberger, M. Tiemann, H.-J. Schmid, G. Grundmeier, *Appl. Surf. Sci.* **2019**, *475*, 873.

[75] X. Dou, D. Mohan, C. U. Pittman, S. Yang, *Chem. Eng. J.* **2012**, *198-199*, 236.

[76] I. Georgieva, N. Danchova, S. Gutzov, N. Trendafilova, *J. Mol. Model.* **2012**, *18*, 2409.

[77] K. Nakamoto, *Infrared and Raman Spectra of Inorganic and Coordination Compounds*, John Wiley & Sons, Inc, Hoboken, NJ, USA **2008**.

[78] G. V. Jere, M. T. Santhamma, *Inorg. Chim. Acta* **1977**, *24*, 57.

[79] M. Behera, S. Ram, *IOP Conf. Ser.: Mater. Sci. Eng.* **2018**, *330*, 012016.

[80] A. L. Saroj, R. K. Singh, S. Chandra, *Mater. Sci. Eng., B* **2013**, *178*, 231.